How to cite: Angew. Chem. Int. Ed. 2025, e202424269
doi.org/10.1002/anie.202424269

Polymer Chemistry Hot Paper

Self-Assembly of Amorphous 2D Polymer Nanodiscs with Tuneable Size, pH-Responsive Degradation and Controlled Drug Release

Haoxiang Zeng[+], Ping Zeng[+], Jinsu Baek, Byeong-Su Kim, and Markus Müllner**

Abstract: Amphiphilic bottlebrush block copolymers (BBCs) with tadpole-like, coil-rod architecture can be used to self-assemble into functional polymer nanodiscs directly in water. The hydrophobic segments of the BBC were tuned via the ratio of ethoxy-ethyl glycidyl ether (EE) to tetrahydropyranyl glycidyl ether (TP) within the grafted polymer sidechains. In turn, this variation controlled the sizes, pH-responsiveness, and drug loading capacity of the self-assembled nanodiscs. Notably, as EE exhibited faster hydrolysis than TP, the nanodiscs featured variable degradation rates under mild acidic conditions, aiding small molecule release and time-dependent and complete degradation of discs into fully water-soluble copolymers. The nanodiscs demonstrated biocompatibility and cellular uptake by breast cancer cells, underscoring their potential development into drug delivery systems.

Two-dimensional nanomaterials draw considerable interest in many fields,[1–5] due to their unique properties attributed to their morphology, increased surface area and high aspect ratio, mechanical stability, and conductivity. Applications in electronics,[6–8] catalysis,[9–11] membranes[12–14] are ubiquitous and, predominantly, make use of well-established synthesis protocols for inorganic and hybrid 2D materials. Soft matter-based 2D nanomaterials are, however, highly desirable in nanomedicine and biomedical applications, with one of the most prominent discoidal nanomaterials being lipid nanodiscs.[14,15] Polymer nanodiscs in this context are highly anticipated as their tunable properties and morphology would bring favorable attributes in terms of in vivo fate, and targeting and delivery applications.[16–18] The most stubborn roadblock remains the lack of suitable and reliable fabrication approaches to yield polymer nanodiscs. Having to overcome the intrinsic propensity to reduce interfacial energy, polymer self-assembly rarely leads to shape-anisotropic planar morphologies.[19,20] Early works in this realm indicated that boosting intermolecular forces between self-assembled polymers may allow the flattening of micelles.[21–23] Periodic success has also been seen in multi-component systems (mostly in organic media),[24] using small molecules,[25] solvent gradients,[26] or copolymer mixtures[27] to tune interfacial energies. In recent years, crystallization-driven self-assembly (CDSA) and, in particular, living CDSA, have partially addressed the synthetic issue by providing a reliable workhorse to crystallize block copolymers into 2D materials, such as platelets.[28–30] Living CDSA allows for precise control over particle size and morphology through chain extension processes, enabling the generation of uniform, anisotropic materials with predictable dimensions and exceptional reproducibility.[31,32] Given that CDSA requires crystalline core-forming domains for it to work and to impart stability, in the context of nanomedicine, CDSA is limited to a handful of polymers (mostly PLA and PCL)[33–35] and typically features an inaccessible crystalline core, thus presenting a significant hurdle for effective drug delivery applications.[36–38]

To achieve a 2D assembly using fully amorphous copolymers, a different driving force is required.[39] Inspired by how rod-coil polymers can be used to facilitate planar stacking,[40–42] we have recently shown that polymer topology can be used to rigidify segments of a block copolymer to yield polymer nanodiscs directly in water.[43] Herein, we prove our hypothesis that using a tadpole-like copolymer architecture can provide a universal approach to self-assembling polymer nanodiscs. Amphiphilic copolymers composed of a linear coil-block and a bottlebrush rod-block can, akin to linear rod-coil copolymers, pack into 2D sheets (Scheme 1). Thus, we synthesized a series of chemically distinct poly(ethoxyethyl glycidyl ether-*ran*-tetrahydropyranyl glycidyl ether)s, P(EE-*ran*-TP)s, to graft as sidechains to form a bottlebrush segment with comparable size but varied chemical properties. As different EE/TP ratios produce polymers with varied glass transition temperature (T_g), hydrophobicity, and susceptibility to hydrolysis,[44] we

[*] H. Zeng,[+] P. Zeng,[+] A/Prof. M. Müllner
Key Centre for Polymers and Colloids, School of Chemistry
The University of Sydney
Sydney, 2006 NSW, Australia
E-mail: markus.muellner@sydney.edu.au

J. Baek, Prof. B.-S. Kim
Department of Chemistry
Yonsei University
Seoul, 03722, Korea
E-mail: bskim19@yonsei.ac.kr

A/Prof. M. Müllner
The University of Sydney Nano Institute (Sydney Nano)
The University of Sydney
Sydney, 2006 NSW, Australia

[+] H. Zeng and P. Zeng contributed equally.

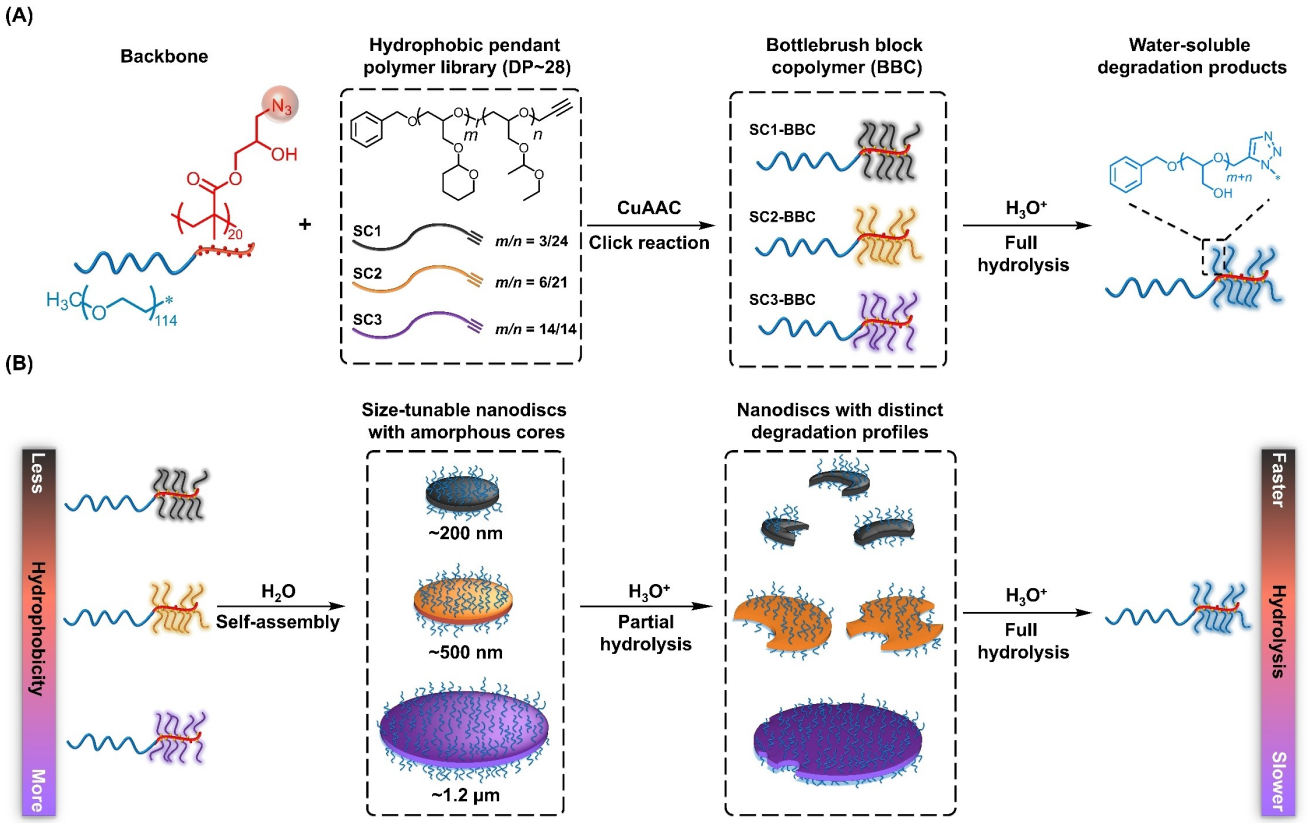

Scheme 1. (A) General synthetic route toward amphiphilic coil-rod BBCs, (B) enabling the self-assembly of amorphous nanodiscs with controllable core functionality and degradation.

could systematically influence the outcome of the self-assembly in terms of particle size (diameter between 0.2–1.2 µm) and physicochemical properties (particle stability, degradation, drug release), while guaranteeing to produce polymer nanodiscs. Additionally, we evaluated the cytotoxicity and cellular uptake of these nanodiscs using the MDA-MB-231 breast cancer cell line, a widely used in vitro model for studying triple-negative breast cancer (TNBC),[45] thereby highlighting their potential as future drug delivery systems.

The synthesis of pH-responsive, tadpole-like BBCs was achieved by selectively grafting poly(glycidyl ether) sidechains onto one block of a diblock copolymer backbone. The diblock copolymer polymer backbone PEG_{114}-*block*-$(PGMA\text{-}N_3)_{20}$ was prepared through reversible addition-fragmentation chain-transfer (RAFT) polymerization and subsequent reaction with sodium azide. Detailed synthesis protocols and characterization can be found in the Supporting Information (Schemes S1 and Figures S1–S6). As sidechains, three copolymer glycidyl ethers with alkyne terminal groups have been prepared via anionic ring-opening polymerization and subsequent post polymerization modification (Schemes S2–S3), featuring a random distribution of EE and TP ratios (sidechains **SC1**: poly(EE_{24}-*ran*-TP_3), **SC2**: poly(EE_{21}-*ran*-TP_6), **SC3**: poly(EE_{14}-*ran*-TP_{14})) but comparable overall degree of polymerization (DP~28). The sidechains were designed to maintain a consistent overall block length while increasing the fractional content of more hydrolytically stable TP from 11 % in SC1 to 50 % in SC3 (Figures S7–S14). To build the final tadpole-like BBCs, SC1, SC2, or SC3 were clicked onto the $(PGMA\text{-}N_3)_{20}$ block of the backbone (Scheme S4–S5).[46,47] The successful synthesis of three unique PEG_{114}-*block*-[$(PGMA\text{-}N_3)_{20}$-*graft*-(P(EE-*ran*-TP)$_{28}$)$_{15}$] (SC-BBC) was confirmed by ^{1}H nuclear magnetic resonance (NMR) spectroscopy (Figures S15–S17) and size exclusion chromatography (SEC) (Figure S18 and Figure S21) analyses. The grafting efficiency of the click reaction, as calculated from NMR, was around 75 %, irrespective of sidechain composition. The efficiency is limited by several factors, including the steric demand of the sidechains, chain folding within the bottlebrush architecture, and the inherent bulkiness of the grafted polymers.[48–50] Given that all three sidechains have nearly identical length, no significant differences were expected.

The BBCs are amphiphilic and feature a hydrophilic linear PEG block and a hydrophobic bottlebrush block. The linear PEG will act like a coil, while the rigidified bottlebrush will act more like a rod polymer. Linear rod-coil copolymers have been demonstrated to achieve 2D self-assembly, for example, via crystallization.[51] Our BBC design borrows from this concept but achieves the rod-like character through topology and conformational changes in the densely grafted bottlebrush segment (75 % grafting efficiency),[52] allowing us to attain rod-coil BBCs capable of

planar packing not driven by crystallization. This further allows us to vary the brush composition without affecting the overall rod-coil architecture. The self-assembly of these amphiphilic BBCs is then somewhat independent of the chemistry of the core-forming block (except it needs to be hydrophobic to promote self-assembly in aqueous solution). This allows us to study the influence of hydrophobicity within the core-forming rod segments, as the EE/TP ratio will determine the overall degree of hydrophobicity of the sidechains.

We postulated that by designing a specific tadpole-like polymer architecture, i.e., the ratio of coil and rod segment, we should be able to achieve 2D self-assembly irrespective of the nature of the bottlebrush core chemistry. In fact, all BBCs have self-assembled directly into nanoscale discs in water (Figure 1 and Figures S22–S23). In comparison, we have synthesized SC2-BBC with 45 % grafting efficiency (Figures S19–S20) to investigate how molecular architecture influences the self-assembly process of BBCs. The reduced grafting efficiency was designed to decrease the rigidity and bending energy of the bottlebrush segments, which consequently drives the BBCs to self-assemble into vesicles rather than nanodiscs (Figure S24). Our results underscore the critical role of the grafting density and block rigidity in dictating the self-assembly behavior of BBCs, highlighting how subtle changes in molecular architecture can lead to distinct nanostructures.

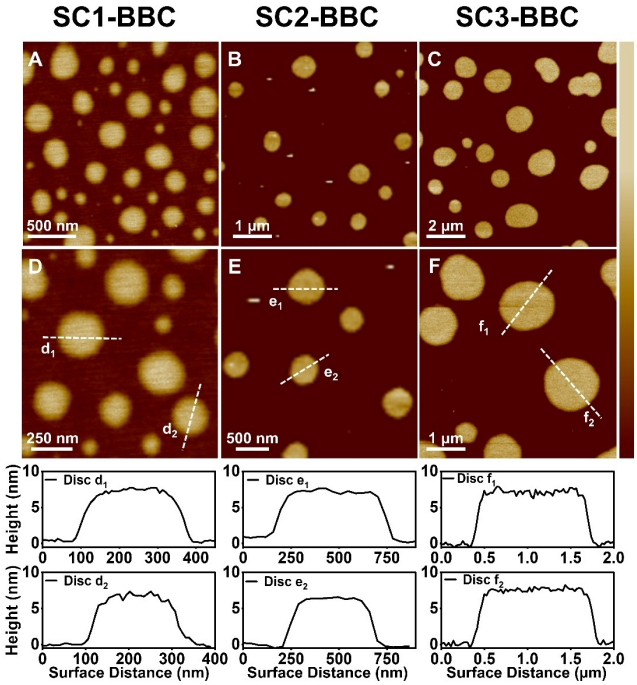

Figure 1. Atomic force microscopy (AFM) height image of self-assembled nanodiscs formed by (A) SC1-BBC, (B) SC2-BBC, and (C) SC3-BBC; (D–F) Zoomed in AFM height images above from (A–C) including cross-sectional analysis across selected nanodiscs. AFM z-scale: −5 to 10 nm.

By gradually increasing the hydrophobicity of grafted poly(EE-*ran*-TP)s, the self-assembled discs exhibited growing diameters, with SC1-BBC nanodiscs ~200 nm, SC2-BBC nanodiscs ~500 nm, and SC3-BBC nanodiscs reached >1 μm, as summarized in Table 1. The varying diameters of the nanodiscs can be attributed to the differences in the hydrophobic interactions among the polymer sidechains, where a higher TP content correlates with increased hydrophobicity, promoting the formation of larger self-assembled structures due to the enhanced aggregation of hydrophobic domains. The uniform thickness across all nanodisc variants (~8 nm) indicated a consistent packing density and polymer orientations within the nanodisc structure, which remains relatively unchanged by varying the composition of the sidechains. However, the ability to adjust the average disc diameter by varying the EE/TP ratio highlights the importance of hydrophobicity in the rod segment and, in addition, enables a simple means to tailor not only the size of discs but also their functionality. Each poly(glycidyl ether) copolymer is pH-sensitive and undergoes a hydrophobic-to-hydrophilic transition in acidic environments. However, the rate of this change is composition-dependent, with the order of increasing stability towards acid hydrolysis being SC1 < SC2 < SC3, in concert with our recent study.[53] Finally, the critical disc-formation concentration (CDC) of SC-BBCs was examined using dynamic light scattering (DLS) and transmission electron microscopy (TEM) (Figures S25–S27). For SC1-BBC and SC2-BBC, stable nanodiscs were observed at concentrations above 0.25 mg/mL. SC3-BBC, with the increased hydrophobicity of the bottlebrush segment, exhibited a lower CDC, forming stable nanodiscs more readily at lower concentrations (above 0.1 mg/mL).

To investigate the pH-dependent stability of prepared nanodiscs, we loaded pyrene as a probe into the core domain (Figure S28). The fluorescence intensity ratio at 336 nm to 333 nm (I_{336}/I_{333}) of pyrene is solvochromatic and, hence, can be used to assess microenvironmental changes,[54,55] and in our case, offer insights into the stability

Table 1: Characterization data on BBCs and their corresponding nanodiscs.

	Bottlebrush sidechains Composition (NMR)[a]	T_g (°C)	Grafting Efficiency (%)[a]	BBCs $M_{n,NMR}$ (kg/mol)[a]	$M_{n,SEC}$ (kg/mol)[b]	$Đ$[b]	Nanodiscs Disc diameter (nm)[c]
SC1-BBC	P(EE_{24}-*ran*-TP_3)	−57.6	75	70.6	68.4	1.15	193 ± 70
SC2-BBC	P(EE_{21}-*ran*-TP_6)	−52.8	75	72.1	57.1	1.17	455 ± 85
SC3-BBC	P(EE_{14}-*ran*-TP_{14})	−42.5	75	75.1	49.7	1.17	1120 ± 310

[a] Determined by ^{1}H NMR spectroscopy using end group analysis; [b] Determined by DMAc-SEC with PMMA calibrations; [c] Determined by AFM with the results expressed as means ± SD of particles presented in Figure 1A–1C.

and structural integrity of the nanodiscs. Under neutral conditions, we attested increased stability to all the nanodiscs as their I_{336}/I_{333} values remained largely unchanged, in the case of SC3-BBC even over a 60-day period (Figures S29–S31). In all cases, the nanodisc structure remained intact for the monitoring period. However, once the nanodiscs were introduced into an acidic environment, a more pronounced shift in their fluorescence analysis was evident (Figures S29–S31). This was primarily driven by the accelerated hydrolysis of the EE and TP segments, leading to a significant reduction in their I_{336}/I_{333} values and indicating the degradation (i.e., disassembly) of the nanodiscs (Figure 2). The degradation profile seems to occur in three distinct stages (Figure 3). Initially (Stage I), their I_{336}/I_{333} values remained relatively stable, indicating nanodiscs have preserved their structural integrity in the acidic environment. Upon further hydrolysis, a gradual decrease in their I_{336}/I_{333} values was observed (Stage II), indicating a hydrolysis-induced structural breakdown of nanodiscs, which consequently exposes pyrene to a more polar environment. Finally (Stage III), the nanodiscs are no longer stable and disintegrate, leaving pyrene exposed to water and leading to a stabilized I_{336}/I_{333} ratio.[55] With progressing hydrolysis, the remaining disc fragments gradually degrade into fully water-soluble macromolecules: PEG-*block*-[polyglycidol].

DLS and TEM analyses further corroborate the expected hydrodynamic size changes and morphology transformations at selected time points (Figure 3 and Figures S32–S37). In all cases, only minor size changes were observed from their DLS traces during the initial degradation stage (Stage I), with TEM suggesting that the initial degradation predominantly stems from the nanodisc periphery. This degradation pattern aligns well with the initial stability observed in the pyrene fluorescence studies, where the core environment around the pyrene molecules remained relatively unchanged due to its encapsulation within the nanodisc cores. As the hydrolysis progressed, the cumulative degradation reached a threshold where the nanodiscs could no longer maintain their integrity and started to disassemble into smaller fragments. This structural breakdown facilitated a greater influx of the acidic buffer solution into the core regions, significantly altering the microenvironment around the pyrene molecules. This alteration was quantitatively evidenced by a marked decline in their I_{336}/I_{333} fluorescence intensity ratio, indicating the

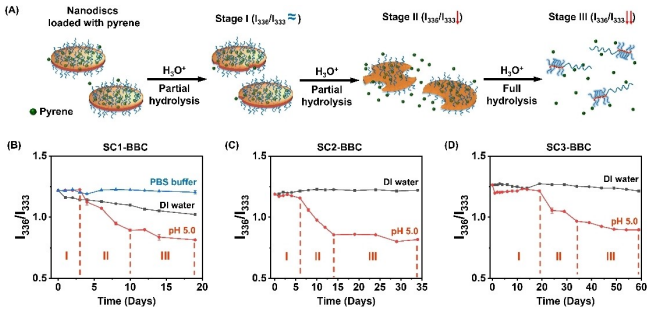

Figure 2. (A) Schematic representation of using pyrene to monitor the degradation process of nanodiscs. Fluorescence intensity ratio at 336 nm to 333 nm (I_{336}/I_{333}) of encapsulated pyrene molecules in (B) SC1-BBC, (C) SC2-BBC, and (D) SC3-BBC nanodiscs over time under neutral and acidic conditions. The results were expressed as means ± SD, $n = 3$ independent replicates.

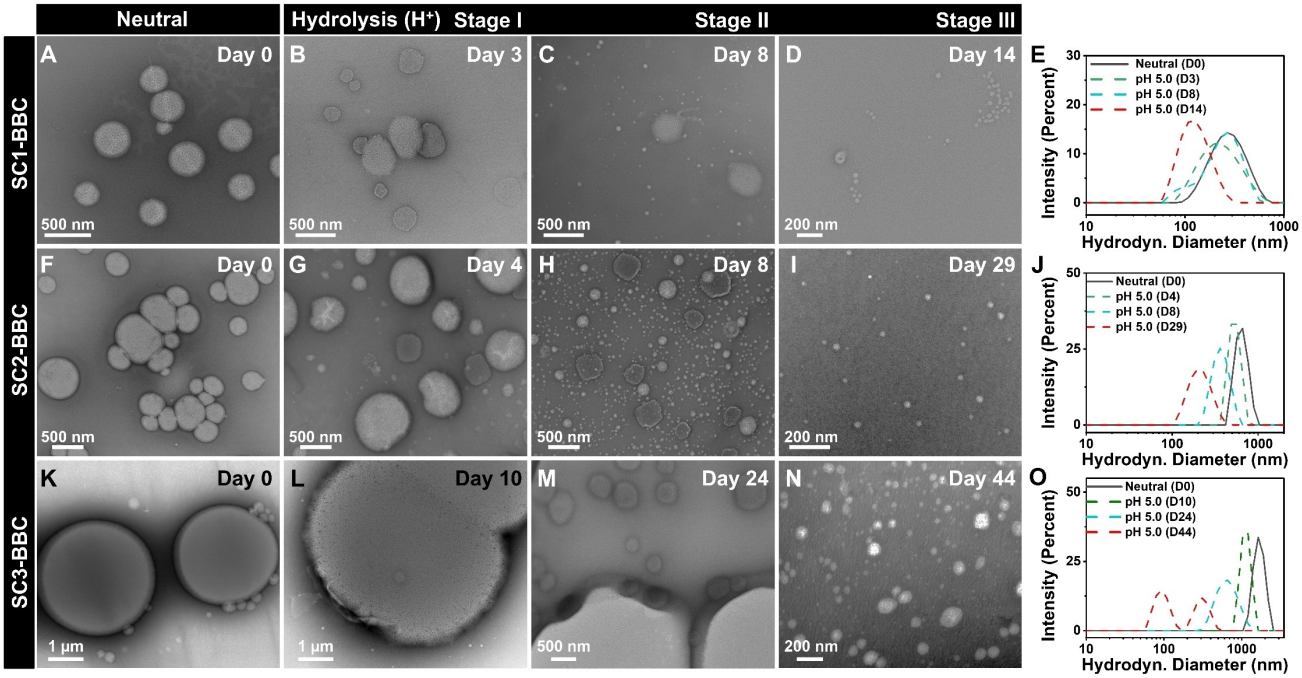

Figure 3. Representative TEM images (negative stain) of nanodiscs at different degradation stages determined from fluorescence kinetic studies and the DLS measurements of their size distributions: (A–E) SC1-BBC, (F–J) SC2-BBC, (K–O) SC3-BBC.

increased microenvironment polarity as the degradation proceeded.

Notably, the degradation kinetics of nanodiscs varied significantly with different EE/TP compositions; while SC1-BBC nanodiscs exhibited the fastest degradation, SC3-BBC experienced the slowest. The variation can be attributed to their differences in hydrophobicity and particle sizes. SC1-BBC nanodiscs, with a higher proportion of rapidly hydrolyzing EE segments, were more susceptible to acidic conditions, leading to a faster structural breakdown and degradation of nanodiscs. In contrast, SC2-BBC and SC3-BBC nanodiscs, characterized by a larger proportion of slowly hydrolyzing TP segments, exhibited enhanced resistance to hydrolysis, thus presenting a slower degradation process. Furthermore, the smallest sizes of SC1-BBC nanodiscs likely contributed to their increased surface-to-volume ratio, accelerating their hydrolysis and degradation processes. The degradation kinetics of nanodiscs can be finely tuned by altering the composition and ratio of EE/TP, offering insights into the design of responsive nanocarrier systems.

pH-responsive polymers have been widely explored as drug carriers due to their unique ability to undergo structure or property changes in response to the pH variations typically found between healthy and diseased tissues.[56–58] We assessed our nanodiscs as potential drug carriers through the encapsulation and subsequent release of the widely studied doxorubicin (DOX) (Figure 4 and Figure S38). The encapsulation efficiency and drug loading content (in wt%), respectively, were: SC1-BBC (18%, 9%), SC2-BBC (15%, 7.5%), SC3-BBC (11%, 5.5%) (Figure S39). Such loading capacity matches established systems based on liposomes and linear polymers.[59,60] Under neutral conditions, stable nanodiscs showed limited premature drug leakage: 8.8 ± 0.4 wt% (SC1-BBC), 5.9 ± 0.4 wt% (SC2-BBC), and 1.9 ± 0.3 wt% (SC3-BBC). The amorphous core acts as a hydrophobic depot, whereby the increase in hydrophobicity and T_g from SC1 to SC3 prevent diffusion additionally. A marked increase in DOX release was observed in acidic environment when the acid-labile cores start to switch to hydrophilic: 69.3 ± 3.7 wt% (SC1-BBC), 54.7 ± 2.7 wt% (SC2-BBC), 24.5 ± 3.2 wt% (SC3-BBC). The different release profiles between the nanodiscs stem from the varying ratios of EE to TP. SC1-BBC contains the highest proportion of the more rapidly hydrolyzing EE segments, and hence release DOX fastest during core degradation. Conversely, SC3-BBC contains the highest proportion of the slowly hydrolyzing TP segments, hence leading to the slowest release rate, due to the slow switch toward hydrophilicity, but also the prolonged stability of the disc itself.

Biocompatibility is a critical factor when considering materials as drug carriers. To assess the biocompatibility of our nanodiscs, MTT assays were performed using MDA-MB-231 cells. The nanodiscs demonstrated biocompatibility, maintaining cell viability above 80% at all tested concentrations after 24 hours of incubation (Figure 5A). Furthermore, cellular uptake studies, conducted with Cy5-labelled nanodiscs, revealed significant internalization into cells after 6 and 24 hours, as evidenced by fluorescence signals in Confocal Laser Scanning Microscopy (CLSM) images (Fig-

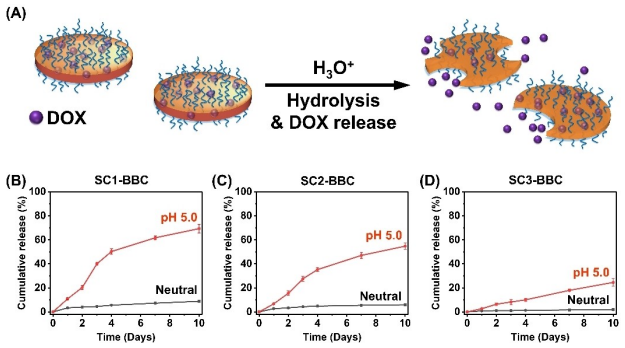

Figure 4. (A) Schematic representation of the release of encapsulated DOX molecules from the degradation of polymer nanodiscs; (B–D) Release profile of encapsulated DOX molecules of SC1-BBC discs, SC2-BBC discs, and SC3-BBC discs under neutral and acidic (pH 5.0) conditions. The results were expressed as means ± SD, $n = 3$ independent replicates.

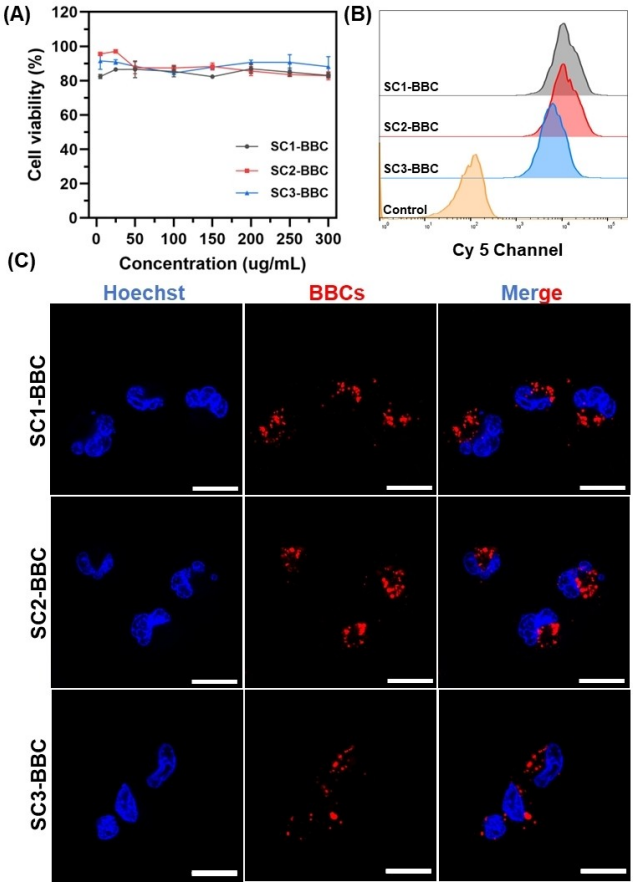

Figure 5. (A) Viability of MDA-MB-231 cells after incubation with Cy5-labelled nanodiscs at different concentrations at 37 °C for 24 h. Data are presented as mean ± SD, n = 3 independent replicates. (B) Flow cytometry analysis of MDA-MB-231 cells incubated with Cy5-labelled nanodiscs at 37 °C for 24 h. (C) CLSM images of MDA-MB-231 cells incubated with Cy5-labelled nanodiscs at 37 °C for 24 h. Scale bar: 20 μm; nucleus: blue; nanodiscs: red.

ure 5C and Figure S40A). Notably, SC1-BBC and SC2-BBC exhibited stronger fluorescence compared to SC3-BBC, likely due to their smaller particle sizes, which enhances cellular uptake. These findings were further confirmed by flow cytometry analysis, which exhibited differences in uptake levels among the nanodisc variants (Figure 5B and Figure S40B). These results reinforce the potential of our nanodiscs as a versatile platform for future drug delivery applications.

In conclusion, this study highlights the benefit of using bottlebrush copolymers in materials science, which is rapidly becoming its own field, owing the unique properties of these highly branched macromolecules. Especially in the context of self-assembly, molecular bottlebrushes provide fast assembly kinetics, impart increased stability, and allow for compartmentalization.[61,62] In our current work, we have successfully prepared a series of BBCs with unique tadpole-like architecture by tuning the EE/TP ratio of grafted polymer sidechains. Through direct self-assembly of such BBCs in water, polymer nanodiscs with customizable sizes and degradation kinetics can be prepared, whereby increased levels of EE degraded corresponding nanodiscs faster. Specifically, the degradation started from the nanodisc periphery and gradually led to the complete disassembly of nanodiscs into fully water-soluble copolymers. Additionally, the nanodiscs demonstrated efficient drug encapsulation, pH-responsive release of DOX, exhibited biocompatibility and were able to be taken up by cancer cells. We anticipate the strategy developed in this work will serve as a functional platform to fabricate polymer nanodiscs with controllable physiochemical properties and develop advanced drug delivery systems.

Supporting Information

Materials, methods, and supporting results, including polymer characterisation (NMR, SEC, differential scanning calorimetry - DSC, Fourier transform infrared spectroscopy - FTIR, TEM, AFM), hydrolysis studies (DLS, TEM, fluorescence spectroscopy) and in vitro studies (plate reader, CLSM, flow cytometry). The authors have cited additional references within the Supporting Information.[63]

Acknowledgements

This research was facilitated by access to Sydney Analytical, a core research facility at the University of Sydney. The authors acknowledge the technical and scientific assistance from Sydney Microscopy & Microanalysis, The University of Sydney node of Microscopy Australia and Sydney Cytometry. The authors thank Prof. Chiara Neto for providing access to atomic force microscopes and the Key Centre for Polymers and Colloids (KCPC) for access to equipment. The authors thank Prof. Elizebeth New for providing the cancer cell line. H. Z. and P. Z. are grateful recipients of Postgraduate Research Scholarships from the University of Sydney. J. B. and B.-S. K. were supported by the National Research Foundation of Korea (NRF-2021R1A2C3004978). M. M. acknowledges the Australian Research Council for a Future Fellowship (FT200100185) and Discovery Project (DP220100452), respectively. M. M. is a grateful recipient of a University of Sydney Research Accelerator (SOAR) Prize. Parts of this work were enabled through a USyd-Yonsei Partnership Collaboration Award (PCA). Open Access publishing facilitated by The University of Sydney, as part of the Wiley - The University of Sydney agreement via the Council of Australian University Librarians.

Conflict of Interest

The authors declare no conflict of interest.

Data Availability Statement

The data that support the findings of this study are available from the corresponding author upon reasonable request.

Keywords: molecular polymer bottlebrushes · polymer nanodiscs · drug delivery system · pH-responsiveness

[1] X. Zhuang, Y. Mai, D. Wu, F. Zhang, X. Feng, *Adv. Mater.* **2015**, *27*, 403–427.
[2] N. Baig, *Composites Part A* **2023**, *165*, 107362.
[3] D. Chimene, D. L. Alge, A. K. Gaharwar, *Adv. Mater.* **2015**, *27*, 7261–7284.
[4] Y. Wang, L. Wang, X. Zhang, X. Liang, Y. Feng, W. Feng, *Nano Today* **2021**, *37*, 101059.
[5] C. Tan, X. Cao, X. J. Wu, Q. He, J. Yang, X. Zhang, J. Chen, W. Zhao, S. Han, G. H. Nam, M. Sindoro, H. Zhang, *Chem. Rev.* **2017**, *117*, 6225–6331.
[6] S. Manzoor, M. Talib, S. M. Novikov, A. V. Arsenin, V. S. Volkov, P. Mishra, *ACS Sens.* **2023**, *8*, 3435–3447.
[7] S. Farokhi, M. Roushani, H. Hosseini, *Electrochim. Acta* **2020**, *362*, 137218.
[8] Z. Meng, R. M. Stolz, L. Mendecki, K. A. Mirica, *Chem. Rev.* **2019**, *119*, 478–598.
[9] W. Liu, Y. Wang, K. Qi, Y. Wang, F. Wen, J. Wang, *J. Alloys Compd.* **2023**, *933*, 167789.
[10] X. Chen, S. Lv, H. Gu, H. Cui, G. Liu, Y. Liu, Z. Li, Z. Xu, J. Kang, G. Teobaldi, L.-M. Liu, L. Guo, *J. Am. Chem. Soc.* **2024**, *146*, 13527–13535.
[11] H. Jin, C. Guo, X. Liu, J. Liu, A. Vasileff, Y. Jiao, Y. Zheng, S. Z. Qiao, *Chem. Rev.* **2018**, *118*, 6337–6408.
[12] F. Hagn, M. Etzkorn, T. Raschle, G. Wagner, *J. Am. Chem. Soc.* **2013**, *135*, 1919–1925.
[13] F. Hagn, M. L. Nasr, G. Wagner, *Nat. Protoc. 2018 13:1* **2017**, *13*, 79–98.
[14] I. G. Denisov, S. G. Sligar, *Chem. Rev.* **2017**, *117*, 4669–4713.
[15] L. Jing, K. Li, H. Yang, P. Y. Chen, *Mater. Horiz.* **2020**, *7*, 54–70.
[16] T. Ravula, N. Z. Hardin, A. Ramamoorthy, *Chem. Phys. Lipids* **2019**, *219*, 45–49.
[17] M. D. Farrelly, L. L. Martin, S. H. Thang, *Chem. Eur. J.* **2021**, *27*, 12922–12939.
[18] E. Blanco, H. Shen, M. Ferrari, *Nat. Biotechnol. 2015 33:9* **2015**, *33*, 941–951.

[19] C. Wang, C. Siu, J. Zhang, J. Fang, *Nano Res.* **2015**, *8*, 2445–2466.
[20] Z. Wang, Y. Mu, D. Lyu, M. Wu, J. Li, Z. Wang, Y. Wang, *Curr. Opin. Colloid Interface Sci.* **2022**, *61*, 101608.
[21] D. Richter, D. Schneiders, M. Monkenbusch, L. Willner, L. J. Fetters, J. S. Huang, M. Lin, K. Mortensen, B. Farago, *Macromolecules* **1997**, *30*, 1053–1068.
[22] M. Nakano, K. Matsumoto, H. Matsuoka, H. Yamaoka, *Macromolecules* **1999**, *32*, 4023–4029.
[23] L. Yin, M. A. Hillmyer, *Macromolecules* **2011**, *44*, 3021–3028.
[24] H. Zhu, Y. Cui, J. Wang, H. Qiu, *RSC Adv.* **2019**, *9*, 9443–9448.
[25] J. Zhu, S. Zhang, K. Zhang, X. Wang, J. W. Mays, K. L. Wooley, D. J. Pochan, *Nat. Commun.* **2013**, *4*, 2297.
[26] Q. Zhang, H. Fan, L. Zhang, Z. Jin, *Macromolecules* **2020**, *53*, 7025–7033.
[27] S. Chen, B. D. Lechner, A. Meister, W. H. Binder, *Nano Lett.* **2016**, *16*, 1491–1496.
[28] M. Inam, J. R. Jones, M. M. Pérez-Madrigal, M. C. Arno, A. P. Dove, R. K. O'Reilly, *ACS Cent. Sci.* **2018**, *4*, 63–70.
[29] Y. Wei, J. Tian, Z. Zhang, C. Zhu, J. Sun, Z. Li, *Macromolecules* **2019**, *52*, 1546–1556.
[30] R. Deng, X. Mao, S. Pearce, J. Tian, Y. Zhang, I. Manners, *J. Am. Chem. Soc.* **2022**, *144*, 19051–19059.
[31] X. Wang, G. Guerin, H. Wang, Y. Wang, I. Manners, M. A. Winnik, *Science* **2007**, *317*, 644–647.
[32] L. MacFarlane, C. Zhao, J. Cai, H. Qiu, I. Manners, *Chem. Sci.* **2021**, *12*, 4661–4682.
[33] R. M. Van Horn, J. X. Zheng, H. J. Sun, M. S. Hsiao, W. Bin Zhang, X. H. Dong, J. Xu, E. L. Thomas, B. Lotz, S. Z. D. Cheng, *Macromolecules* **2010**, *43*, 6113–6119.
[34] Y. Kwon, H. Ma, K. T. Kim, *Macromolecules* **2022**, *55*, 2768–2776.
[35] X. Zhang, G. Chen, B. Zheng, Z. Wan, L. Liu, L. Zhu, Y. Xie, Z. Tong, *Biomacromolecules* **2023**, *24*, 1032–1041.
[36] M. Shaheen-Mualim, N. Kutner, S. Farah, *Polym. Adv. Technol.* **2022**, *33*, 3797–3799.
[37] T. Madheswaran, M. Kandasamy, R. J. Bose, V. Karuppagounder, *Drug Discovery Today* **2019**, *24*, 1405–1412.
[38] T. Casalini, F. Rossi, A. Castrovinci, G. Perale, *Front. Bioeng. Biotechnol.* **2019**, *7*, 483145.
[39] E. R. L. Brisson, M. J. H. Worthington, S. Kerai, M. Müllner, *Chem. Soc. Rev.* **2024**, *53*, 1984–2021.
[40] T. W. Schleuss, R. Abbel, M. Gross, D. Schollmeyer, H. Frey, M. Maskos, R. Berger, A. F. M. Kilbinger, *Angew. Chem. Int. Ed.* **2006**, *45*, 2969–2975.
[41] X. Lin, X. He, C. Hu, Y. Chen, Y. Mai, S. Lin, *Polym. Chem.* **2016**, *7*, 2815–2820.
[42] X. Jin, F. Wu, J. Lin, C. Cai, L. Wang, J. Chen, L. Gao, *Langmuir* **2021**, *37*, 3148–3157.
[43] H. Zeng, X. Liang, D. A. Roberts, E. R. Gillies, M. Müllner, *Angew. Chem. Int. Ed.* **2024**, *63*, e202318881.
[44] J. Song, E. Hwang, Y. Lee, L. Palanikumar, S. H. Choi, J. H. Ryu, B. S. Kim, *Polym. Chem.* **2019**, *10*, 582–592.
[45] K. M. Aw Yong, P. J. Ulintz, S. Caceres, X. Cheng, L. Bao, Z. Wu, E. M. Jiagge, S. D. Merajver, *Sci. Rep.* **2020**, *10*, 5781.
[46] P. Zhao, Y. Yan, X. Feng, L. Liu, C. Wang, Y. Chen, *Polymer (Guildf)* **2012**, *53*, 1992–2000.
[47] Y. Yan, Y. Shi, W. Zhu, Y. Chen, *Polymer (Guildf)* **2013**, *54*, 5634–5642.
[48] B. Jiang, L. Zhang, J. Yan, Q. Huang, B. Liao, H. Pang, *J. Polym. Sci. Part A* **2014**, *52*, 2442–2453.
[49] N. K. Obhi, D. M. Peda, E. L. Kynaston, D. S. Seferos, *Macromolecules* **2018**, *51*, 2969–2978.
[50] L. Xiao, J. Li, G. Peng, G. Huang, *React. Funct. Polym.* **2020**, *156*, 104736.
[51] F. Xu, J. Zhang, P. Zhang, X. Luan, Y. Mai, *Mater. Chem. Front.* **2019**, *3*, 2283–2307.
[52] R. Wang, Q. Wei, W. Sheng, B. Yu, F. Zhou, B. Li, *Angew. Chem. Int. Ed.* **2023**, *62*, e202219312.
[53] J. Baek, N. Song, B. Yoo, D. Lee, B. S. Kim, *J. Am. Chem. Soc.* **2024**, *146*, 13836–13845.
[54] K. Ayyavoo, P. Velusamy, *New J. Chem.* **2021**, *45*, 10997–11017.
[55] H. J. Lee, S. H. Kwon, K. S. Jang, *RSC Adv.* **2016**, *6*, 86361–86372.
[56] N. Deirram, C. Zhang, S. S. Kermaniyan, A. P. R. Johnston, G. K. Such, *Macromol. Rapid Commun.* **2019**, *40*, 1800917.
[57] S. R. Mane, A. Sathyan, R. Shunmugam, *ACS Appl. Nano Mater.* **2020**, *3*, 2104–21117.
[58] H. Ding, P. Tan, S. Fu, X. Tian, H. Zhang, X. Ma, Z. Gu, K. Luo, *J. Controlled Release* **2022**, *348*, 206–238.
[59] A. Kowalczuk, R. Trzcinska, B. Trzebicka, A. H. E. Müller, A. Dworak, C. B. Tsvetanov, *Prog. Polym. Sci.* **2014**, *39*, 43–86.
[60] S. Dattani, X. Li, C. Lampa, D. Lechuga-Ballesteros, A. Barriscale, B. Damadzadeh, B. R. Jasti, *Int. J. Pharm.* **2023**, *631*, 122464.
[61] T. Pelras, C. S. Mahon, M. Müllner, *Angew. Chem. Int. Ed.* **2018**, *57*, 6982–6994.
[62] M. Müllner, *Chem. Commun.* **2022**, *58*, 5683–5716.
[63] A. J. Gormley, J. Yeow, G. Ng, Ó. Conway, C. Boyer, R. Chapman, *Angew. Chem. Int. Ed.* **2018**, *57*, 1557–1562.

Manuscript received: December 11, 2024
Accepted manuscript online: January 10, 2025
Version of record online: ■■, ■■

Communication

Polymer Chemistry

H. Zeng, P. Zeng, J. Baek, B.-S. Kim,*
M. Müllner* ——— **e202424269**

Self-Assembly of Amorphous 2D Polymer Nanodiscs with Tuneable Size, pH-Responsive Degradation and Controlled Drug Release

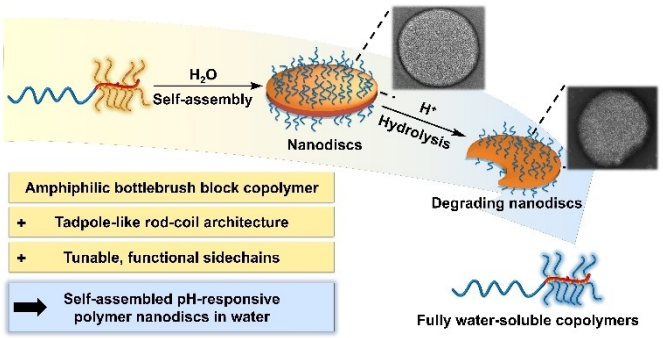

Tadpole-like amphiphilic bottlebrush block copolymers (BBCs) with pH-responsive side chains are synthesized to prepare self-assembled nanodiscs, with sizes from 200 nm to over 1 μm controlled by sidechain compositions. These nanodiscs enter cancer cells, degrade in acidic conditions, with different hydrolysis kinetics, enabling targeted drug release, demonstrating significant potential for therapeutic applications.